Analytical Methods

ROYAL SOCIETY OF CHEMISTRY

TECHNICAL NOTE

View Article Online
View Journal | View Issue

Cite this: *Anal. Methods*, 2025, **17**, 9494

HunStat2 – a simple and low-cost potentiostat with electrochemical impedance spectroscopy capability

Istvan Vamos, [a] Richard Morrison,[b] Sandor Michaletzky[c] and Vilmos Kertesz *[d]

We have developed a low-cost (30 USD), simple do-it-yourself (DIY) potentiostat with cyclic voltammetry (CV), open circuit potential (OCP) and electrochemical impedance spectroscopy (EIS) capability. The HunStat2 potentiostat is based on Analog Devices' AD5941 Analog Front End chip, which significantly simplifies the construction of potentiostats for both direct and alternating current (DC and AC, respectively) techniques. Interested readers are provided with circuit diagrams and a bill of materials to build the potentiostat on their own. In addition, control software is also provided free of charge. The software enables acquisition and visualization of data. In summary, HunStat2 introduces a simple and low-cost DIY potentiostat recommended for both analytical and educational purposes.

Received 17th July 2025
Accepted 21st October 2025

DOI: 10.1039/d5ay01179e

rsc.li/methods

1 Introduction

The primary instruments used to study redox reactions are electrochemical potentiostats. They help researchers investigate reaction mechanisms and kinetics in electrochemical systems.[1] However, commercial potentiostats are typically expensive, often costing several hundred US dollars or more. To address this barrier, various low-cost alternatives have been developed, broadening access to electrochemical experimentation for educators and budget-conscious researchers.[2] These affordable options lower the threshold for participation in both research and education.

Among the different electrochemical techniques, electrochemical impedance spectroscopy (EIS) is one of the most powerful techniques for analyzing electrochemical systems, enabling the separation of simultaneously occurring processes based on their different time constants.[3] This method is particularly useful in the development of electrochemical sensors, as it allows fine-tuning of sensor sensitivity and response time.[4,5]

However, constructing a potentiostat capable of performing EIS is complex, and thus only a few open-source designs exist in the literature besides the more expensive commercial systems. These "do-it-yourself" (DIY) EIS-capable potentiostats are summarized in Table 1.[6–10] Importantly, none of these DIY potentiostats can measure open circuit potential (OCP). EIS performed at the previously measured OCP value allows researchers to investigate the electrochemical impedance of the system in its equilibrium state. This is especially desirable for studying phenomena like corrosion or charge transfer at the electrode–electrolyte interface.[3]

The aim of our work was to develop a low-cost potentiostat featuring OCP and EIS measurements that can be easily constructed and features a no-install, easy-to-use software interface. In this paper, we report on the development of the HunStat2 device capable of cyclic voltammetry (CV), OCP and EIS measurements. The Analog Devices AD5941 chip, introduced a few years ago, integrates key analog and digital components for both direct and alternating current (DC and AC, respectively) electrochemical measurements, supporting amperometry, chronoamperometry, CV, square wave voltammetry, and EIS, making it an excellent choice for low-cost potentiostat construction.[11] HunStat2 utilizes this chip interfaced with a Seeeduino XIAO RP2040 microcontroller,[12] enabling EIS measurements across a frequency range of 0.2 Hz to 200 kHz and the hardware is supported by simple Windows based freeware software. Validation was achieved by comparative measurements with a commercially available potentiostat.

2 Materials and methods

2.1 Chemicals and reagents

Milli-Q Water with an electrical resistivity of >18.2 MΩ cm was used in all experiments. KNO_3 and $K_4Fe(CN)_6$ were obtained from Sigma-Aldrich Kft. (Budapest, Hungary).

2.2 Hardware and software

The AD5941 and XIAO RP2040 chips and the various circuit elements (resistors, capacitors, *etc.*) were purchased from

[a]*Lajos Petrik Vocational Chemistry School, Budapest, Hungary*
[b]*Retired Scientist, Melbourne, Australia*
[c]*Software Developer, Budapest, Hungary*
[d]*Biosciences Division, Oak Ridge National Laboratory, Oak Ridge, USA. E-mail: kerteszv@ornl.gov*

Table 1 Key characteristics of the most relevant DIY potentiostats with EIS capability. LSV: linear sweep voltammetry; CV: cyclic voltammetry; SWV: square wave voltammetry; CA: chronoamperometry; DPV: differential pulse voltammetry; OCP: open-circuit potentiometry

Name	Year	EIS range	Price in USD	Techniques	Communication	Ref.
ABE-STAT	2019	100 kHz–0.1 Hz	105	CV, DPV, EIS	Bluetooth	6
Matsubara	2021	10 kHz–1 Hz	410	CV, SWV, EIS	USB	7
TBISTAT	2022	1 MHz–0.1 Hz	78	EIS	Bluetooth	8
ACEStat	2022	120 kHz–1 Hz	60	LSV, CV, SWV, CA, EIS	USB	9
HELPStat	2024	200 kHz–0.15 Hz	51	EIS	Bluetooth	10
HunStat2	2025	200 kHz–0.2 Hz	30	CV, EIS, OCP	USB	This paper

Table 2 Part numbers and prices (as of May 20, 2025) of the components required for assembling the HunStat2 potentiostat. In addition, USB Type-C cable was purchased locally for ~$2, 10 printed circuit boards (PCBs) were ordered from a local PCB manufacturer for ~ $10 ($1 per piece), and 10 90° 3-pin connectors to connect the SPE electrode to the board were purchased for ~$1 (0.1$-per piece)

Qty	Components	Value	Price in USD	Mouser part no.
1	AD5941 BCPZ	(SOIC)	9.93	584-AD5941BCPZ
1	XIAO RP2040		5.37	713-102010428
3	1206 SMD resistor	10 K (1%)	0.9	71-RCV1206110KFKEA
1	Resistor 1206 SMD	200 (5%)	0.26	71-CRCW1206200RFKEAH
3	Resistor 1206 SMD	0 Ω	0.3	71-CRCW1206-0-E3
12	Capacitor 1206 SMD	100 nF (25 V)	6.0	80-C1206C104K3HAUTO
1	Capacitor 1206 SMD	4.7 μF (25 V)	0.20	80-C1206C479D5HAUTO
4	Capacitor 1206 SMD	470 nF (25 V)	0.72	80-C1206C474K3RAC
1	Capacitor 1206 SMD	220 pF (25 V)	0.19	80-C1206C221J1HAUTO
1	Inductor 1206 SMD	600 (25 V)	0.17	963-FBMJ3216HM600-T
2	Tactile switch SMD	6 × 6 mm	0.34	179-TS046695BK260SMT

Mouser Electronics (Mansfield, TX, USA) to build the HunStat2 potentiostat. Part numbers and prices (as of May 20, 2025) of the components required for assembling the potentiostat are listed in Table 2. Gerber files, Pick-and-Place and bill of materials (BOM) files are deposited in the GitHub repository,[13] which enables the potentiostat to be directly ordered as a fully assembled printed circuit board (PCB).

The schematic diagram, printed circuit boards, the soldered final design of the HunStat2 potentiostat and the photo of the developed potentiostat are shown in Fig. 1 (important: to be able to measure OCP, the reference electrode must be connected to the AIN3 pin on the board; see Fig. S2 in the SI section). Once the hardware is assembled, the next step is to install the required software. The Arduino IDE should first be installed on your computer.[14] The Arduino sketch package is then uploaded to the Seeeduino XIAO RO2040 board. Finally, the Windows graphical user interface (GUI) software, along with the necessary configuration files—HunStat2.exe and HunStat2.ini—is installed to operate the potentiostat. Note that these files may be updated over time as additional electrochemical techniques are integrated. For the most recent versions, see the public GitHub repository[13] and/or please contact the authors. More details on the potentiostat hardware and the freely available software are described in the SI section.

The compliance limits of the HunStat2 system are as follows: a maximum output range of ±2.1 V, the lowest current range of 54 pA (PGA set to gain 1); a minimal potential step of 537.24 μV

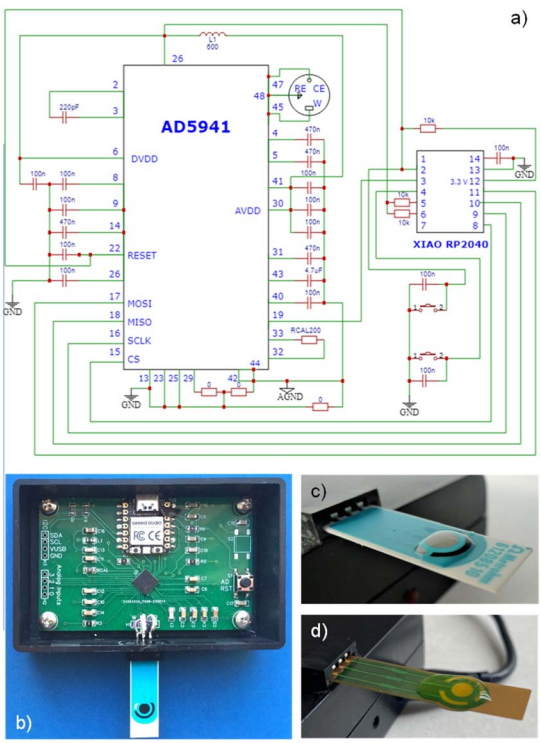

Fig. 1 (a) Schematic diagram, (b) front of the double-sided PCB, and the assembled HunStat2 potentiostat using the (c) Metrohm DS110 carbon screen-printed or (d) Linxens OT5c gold screen-printed electrode.

at the 12-bit DAC; a frequency range of 0.2 Hz to 200 kHz. More details on compliance limits are described in the SI.

2.3 Electrodes

Some of the experiments described below were conducted using a carbon screen-printed electrode (model DS110, DropSens, Llanera, Spain), while others were carried out using a gold screen-printed electrode (Linxens OT5c Gold Electrodes, PN 9X85204FA) provided by Linxens (Ängelholm, Sweden). The electrodes were connected to the board using a 90° 3-pin connector. The three pins of the connector were soldered to the electrical connections of the three electrodes on the board. The central circular spot was used as the working electrode (WE), the right semicircular arc was used as the counter electrode (CE), and the left short connector was used as the reference electrode (RE) (see Fig. 1).

3 Results and discussion

3.1. Validation of the HunStat2 potentiostat

To validate the HunStat2 system, comparative measurements were conducted using the HunStat2 and a commercially available VoltaLab 40 (Radiometer Analytical, Villeurbanne, France). First, a dummy cell was analyzed. The RE and CE were connected (RE-CE), and for the CV measurements, a 500 Ω resistor in series with a 1000 μF capacitor was placed between the WE and RE-CE electrodes, while for the EIS measurements, a 1 kΩ resistor in series with a 10 kΩ resistor and a 680 nF capacitor in parallel was placed between the WE and RE-CE electrodes (note, there is no solution needed). The overlapping curves in Fig. 2 validated the proper operation of the CV (Fig. 2a) and EIS (Fig. 2b) methods using the HunStat2 system. In addition, further validation showed closely matching results of EIS measurements using 5 mM $K_4Fe(CN)_6$/0.1 M KNO_3 solution with both the HunStat2 and the VoltaLab 40 systems and are presented in the SI. Furthermore, CVs recorded for 3–5 mM $K_4Fe(CN)_6$/0.1 M KNO_3 solutions are presented in the SI as well to highlight the CV capability of the system.

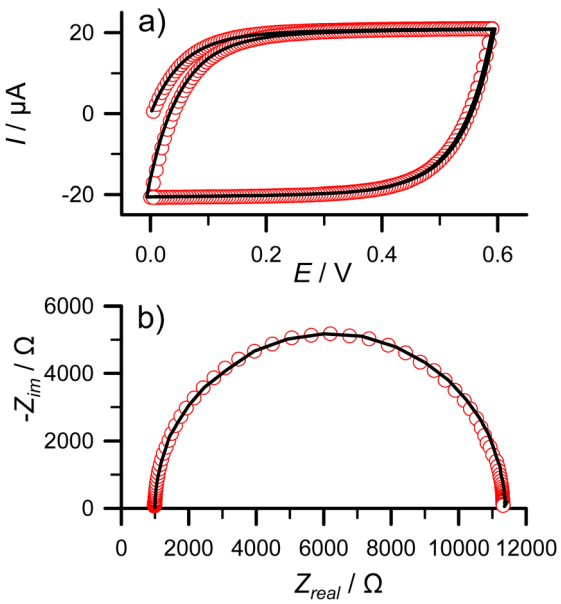

Fig. 2 (a) Cyclic voltammograms and (b) Nyquist plots collected using (red circles) VoltaLab 40 and (black lines) HunStat2 potentiostats recorded under the same conditions with dummy cells ((a) 500 Ω resistor in series with a 1000 μF capacitor, 0 to 0.6 V with 0.1 V s^{-1}; (b) a 1 kΩ resistor in series with a 10 kΩ resistor and 680 nF capacitor in parallel over a frequency range of 10 kHz to 0.2 Hz) with combined reference/counter electrodes. AC amplitude used for EIS was 30 mV.

3.2 EIS measurements at different bias voltages

Measuring impedance at or near the OCP is particularly relevant. For example, in corrosion studies the OCP is the potential that a metal naturally assumes when freely corroding in its environment without any externally applied current or voltage.[3] Performing EIS at the measured OCP value provides conditions that approximate equilibrium, thereby enabling the characterization of the system under circumstances that closely reflect its natural state. Under such conditions, the use of equivalent electrical circuit models, which are generally valid only at or near equilibrium, becomes more appropriate. In summary, carrying out EIS at the measured OCP allows a more reliable assessment of corrosion behaviour while maintaining conditions that remain close to the natural electrochemical state of the system. In practice, OCP was determined first, and EIS was then carried out in a potentiostatic fashion at this potential ($E = E_{OCP}$). This approach does not represent galvanostatic OCP-EIS, but rather potentiostatic EIS at the measured OCP value.

To demonstrate the OCP capability of HunStat2, OCP was measured first in a 5 mM $K_4Fe(CN)_6$/0.1 M KNO_3 solution using a DropSens DS110 carbon screen-printed electrode yielding $E_{OCP} = 0.11$ V. This was followed by recording Nyquist plots at bias voltages of 0 mV (*i.e.* $E = E_{OCP}$), 50 mV and 110 mV over a frequency range of 10 kHz to 0.5 Hz (Fig. 3). At bias voltages greater than 0 mV, the diameter of the semi-circle decreased, indicating changes in the charge transfer resistance (R_{ct}) of the system. These results demonstrate that biasing the electrode moves the system away from equilibrium and causes significant changes in the Nyquist plot (Fig. 3). Measuring EIS at the OCP

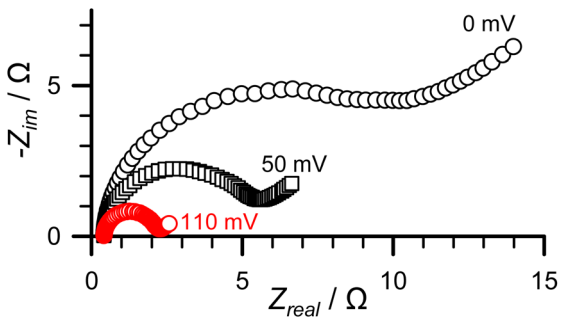

Fig. 3 Nyquist plots collected in a 5 mM $K_4Fe(CN)_6$/0.1 M KNO_3 solution using (black circles) 0 mV, (black squares) 50 mV and (red circles) 110 mV bias voltages over a frequency range of 10 kHz to 0.5 Hz employing a DropSens DS110 carbon screen-printed electrode. AC amplitude used for EIS was 30 mV.

potential, as implemented in HunStat2, therefore provides a straightforward way to interpret Nyquist plots under near-equilibrium conditions.

3.3 Concentration determination using EIS

If an analyte affects electron transfer, double-layer capacitance, or diffusion, then its concentration will influence the impedance response when probing the system using EIS. The equivalent electrical circuit of the reversible electrode reaction of hexacyanoferrate, *i.e.*

$$[Fe(CN_6)]^{4-} \underset{\text{reduction}}{\overset{\text{oxidation}}{\rightleftharpoons}} [Fe(CN_6)]^{3-} + e^- \quad (1)$$

is shown in Fig. 4a. In the circuit, R_u is the ohmic (uncompensated) resistance of the electrolyte between the reference and the working electrodes, R_{ct} is the charge-transfer resistance, C_{dl} is the electrical double layer capacity and Z_W is the Warburg impedance expressing the difficulty of mass transport of the redox species to the electrode surface considering a semi-infinite linear diffusion.[15]

The Warburg impedance can be explained as

$$Z_W = [\sigma\omega^{-1/2} - j(\sigma\omega^{-1/2})] \quad (2)$$

In eqn (2), ω is the angular frequency in rad s^{-1}, j is a complex number equal to $\sqrt{-1}$ and σ can be expressed as

$$\sigma = \frac{2RT}{n^2F^2\sqrt{2Dc}} \quad (3)$$

where R is the gas constant (8.314 J mol^{-1} K^{-1}), T is the temperature in K, n is the number of electrons transferred in the electrochemical reaction, F is Faraday's constant (96 485 C mol^{-1}), D is the diffusion coefficient of the redox couple in cm^2 s^{-1} and c is the concentration of the redox species in mol cm^{-3}. Based on this, the real (Z_{real}) and imaginary ($-Z_{im}$) parts of impedance can be written as

$$Z_{real} = R_u + \frac{R_{ct} + \sigma\omega^{-1/2}}{(\sigma\omega^{1/2}C_{dl} + 1)^2 + \omega^2 C_{dl}^2 (R_{ct} + \sigma\omega^{-1/2})^2} \quad (4)$$

$$-Z_{im} = \frac{\omega C_{dl}(R_{ct} + \sigma\omega^{-1/2})^2 + \sigma^2 C_{dl} + \sigma\omega^{-1/2}}{(\sigma\omega^{1/2}C_{dl} + 1)^2 + \omega^2 C_{dl}^2 (R_{ct} + \sigma\omega^{-1/2})^2} \quad (5)$$

On the other hand, for a reversible reaction like eqn (1), R_{ct} can be derived from the Butler–Volmer equation at small overpotentials as a function of the concentration of the redox species [1]

$$R_{ct} = \frac{RT}{kn^2F^2c} \quad (6)$$

where k is the heterogeneous electron transfer rate constant of the reaction in cm s^{-1} and the other parameters are defined above.

Eqn (6) shows that there is an inverse linear relationship between R_{ct} and the concentration of the redox analyte. To demonstrate this inverse linear relationship, first Nyquist plots were collected using HunStat2 in 3 mM, 4 mM and 5 mM $K_4Fe(CN)_6$/0.1 M KNO_3 solutions using 0 mV bias voltage (E_{OCP} = 0 V; all electrodes were gold) over a frequency range of 10 kHz to 1 Hz employing a Linxens OT5c gold screen-printed electrode (Fig. 4b). These curves were then fitted using eqn (4) and (5) using our separate, in-house developed software specifically written to model the circuit in Fig. 4. Solid lines in Fig. 4b indicate best-fit Nyquist curves with parameters shown in Table 3 (note that HunStat2 is not capable of fitting models. Several software packages are available commercially to model various circuits).

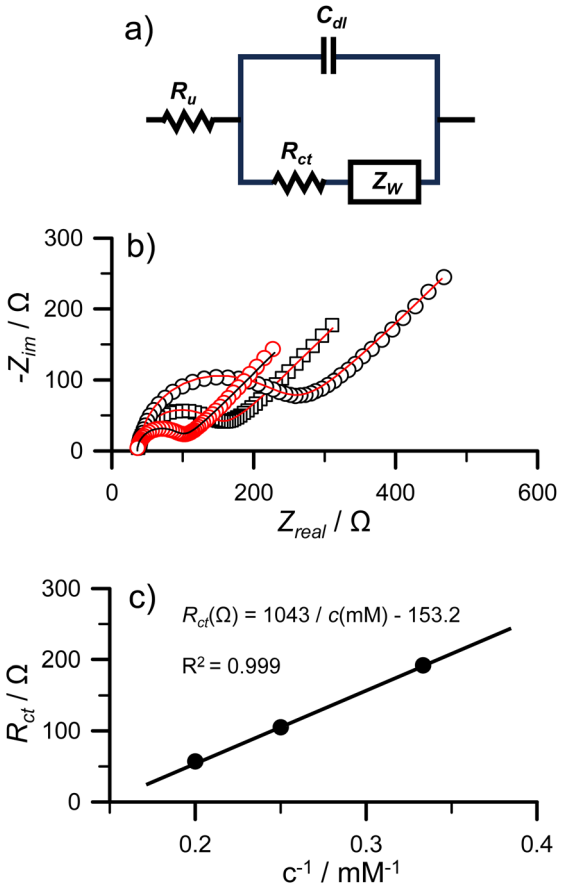

Fig. 4 (a) The equivalent electrical Randles circuit of the reversible electrode reaction of hexacyanoferrate. (b) Nyquist plots collected in (black circles) 3 mM, (black squares) 4 mM and (red circles) 5 mM $K_4Fe(CN)_6$/0.1 M KNO_3 solutions using 0 mV bias voltage (E_{OCP} = 0 V) over a frequency range of 10 kHz to 1 Hz employing a Linxens OT5c gold screen-printed electrode. AC amplitude used for EIS was 30 mV. Solid lines in (b) indicate calculated Nyquist curves using eqn (4) and (5) and Randles circuit in (a) with parameters shown in Table 3. (c) R_{ct} as a function of the reciprocal of $K_4Fe(CN)_6$ concentration (*i.e.* 1/*c*). Linear fit parameters are shown in the figure.

Table 3 Parameters to fit the Nyquist curves in Fig. 4b using eqn (4) and (5) at different analyte concentrations

c mM	R_u Ω	R_{ct} Ω	C_{dl} μF	σ $\Omega^{1/2}$ $\mu F^{-1/2}$
3	39	192	4.0	600
4	37	105	4.0	430
5	36	57	4.0	345

The plot of R_{ct} as a function of $1/c$ is presented in Fig. 4c and shows good linearity (R_{ct} (Ω) = 1043/c (mM) + 153.2, R^2 = 0.999) supporting the inverse linear relationship between R_{ct} and the concentration of the redox analyte as described in eqn (6). This correlation can ultimately be used to determine the concentration of a redox analyte by using a calibration curve such as in Fig. 4c and acquiring the Nyquist plot in an unknown solution using HunStat2.

4 Conclusion

In this paper, we presented HunStat2, a low-cost, easily assembled potentiostat based on an AD5941 chip and an XIAO RP2040 microcontroller, designed for both analytical measurements and educational purposes. Besides CV, the system supports OCP determination and EIS measurements at different bias voltages across a frequency range of 0.2 Hz to 200 kHz. An important feature of HunStat2 is its capability to first determine the OCP and then perform potentiostatic EIS at this potential. While this approach does not represent galvanostatic OCP-EIS, it provides conditions close to equilibrium, which are advantageous for applying equivalent electrical circuit models and for studying processes such as corrosion. In addition, the approximately $30 total cost combined with its minimal assembly time (less than one hour following procurement of the printed circuit board and components) makes this potentiostat easy to assemble and very affordable.

Moreover, to facilitate reproducibility and wider adoption, the design files (Gerber, Pick-and-Place, and BOM) provided in the GitHub repository also allow the device to be ordered in a fully assembled form. The completed instrument interfaces directly with a computer *via* a USB Type-C connection. Furthermore, the hardware is supported by simple Windows-based freeware software. The simple-to-use GUI software boasts several features: potential–current curve plotting for CV, Nyquist and Bode plots for EIS, baseline editing, peak height evaluation, curve smoothing, and the option to export measurement data series. In addition, the GUI is a standalone, single Windows executable file, not requiring any installation and smaller than 1 MB in size. Validation was achieved by comparative measurements with a commercially available potentiostat. In addition, an inverse linear relationship between the charge transfer resistance and the concentration of hexacyanoferrate for its reversible electrode reaction was demonstrated.

Future work will focus on developing WiFi and/or Bluetooth connectivity for remote control applications.

Hazards and safety precautions

CAUTION! Work in rubber gloves and do not pour the remaining solutions down the drain! Always read the MSDS of all used chemicals before using them and follow the federal and local regulations.

Author contributions

Istvan Vamos: conceptualisation; methodology; investigation; formal analysis; writing – review & editing. Richard Morrison: software. Sandor Michaletzky: software. Vilmos Kertesz: project administration; software; visualization; writing – original draft.

Conflicts of interest

The authors report no conflict of interest.

Data availability

The data supporting this article and its availability have been included as part of the supplementary information (SI). Supplementary information: potentiostat hardware, instructions for setting up the Seeeduino XIAO RP2040 in the Arduino IDE and information on the HunStat2 graphical user interface software. See DOI: **https://doi.org/10.1039/d5ay01179e**.

Acknowledgements

The work of VK was sponsored by Oak Ridge National Laboratory, managed by UT-Battelle, LLC, for the U.S. Department of Energy. This manuscript has been authored by UT-Battelle, LLC, under contract DE-AC05-00OR22725 with the US Department of Energy (DOE). The US government retains and the publisher, by accepting the article for publication, acknowledges that the US government retains a nonexclusive, paid-up, irrevocable, worldwide license to publish or reproduce the published form of this manuscript, or allow others to do so, for US government purposes. DOE will provide public access to these results of federally sponsored research in accordance with the DOE Public Access Plan (**https://www.energy.gov/downloads/doe-public-access-plan**).

Notes and references

1 A. J. Bard and L. R. Faulkner, *Electrochemical Methods: Fundamentals and Applications*, Wiley, New York, USA, 2001.
2 I. Vamos and V. Kertesz, *Anal. Methods*, 2024, **16**, 4198–4204, DOI: **10.1039/D4AY00791C**.
3 A. Ch. Lazanas and M. I. Prodromidis, *ACS Meas. Sci. Au.*, 2023, **3**, 162–193, DOI: **10.1021/acsmeasuresciau.2c00070**.
4 M. I. Prodromidis, *Electrochim. Acta*, 2010, **55**, 4227–4233, DOI: **10.1016/j.electacta.2009.01.081**.
5 E. Souteyrand, J. R. Martin and C. Martelet, *Sensor. Actuator. B Chem.*, 1994, **20**, 63–69, DOI: **10.1016/0925-4005(93)01165-Z**.
6 D. M. Jenkins, B. E. Lee, S. Jun, J. Reyes-De-Corcuera and E. S. McLamore, *J. Electrochem. Soc.*, 2019, **166**, B3056–B3065, DOI: **10.1149/2.0061909jes**.
7 Y. Matsubara, *J. Chem.*, 2021, **98**, 3362–3370, DOI: **10.1021/acs.jchemed.1c00228**.
8 F. Burgos-Flórez, A. Rodríguez, E. Cervera, V. Zucolotto, M. Sanjuán and P. J. Villalba, *PLoS One*, 2022, **17**, e0263738, DOI: **10.1371/journal.pone.0263738**.

9 E. W. Brown, M. W. Glasscott, K. Conley, J. Barr, J. D. Ray, L. C. Moores and A. Netchaev, *Anal. Chem.*, 2022, **94**, 4906–4912, DOI: **10.1021/acs.analchem.1c04226**.
10 K. A. Bautista, E. Madsen, S. D. Riegle and J. C. Linnes, *ACS Electrochem.*, 2025, **1**, 386–394, DOI: **10.1021/acselectrochem.4c00052**.
11 **https://www.analog.com/en/products/ad5941.html**, last accessed, 2025.
12 **https://wiki.seeedstudio.com/Seeeduino-XIAO/**, last accessed on, 2025.
13 **https://github.com/hunstat2/HunStat2**, last accessed, 2025.
14 **https://www.arduino.cc**, last accessed, 2025.
15 A. C. Lazanas and M. I. Prodromidis, *ACS Meas. Sci. Au.*, 2023, **3**, 162–193, DOI: **10.1021/acsmeasuresciau.2c00070**.